Proceedings of the Institution of Mechanical Engineers, Part G: Journal of Aerospace Engineering

http://pig.sagepub.com/

Aeroelastic Characteristics of Slender Wing/Bodies with Freeplay Non-Linearities

F Arévalo and P García-Fogeda

Proceedings of the Institution of Mechanical Engineers, Part G: Journal of Aerospace Engineering 2011 225: 347
DOI: 10.1243/09544100JAERO734

The online version of this article can be found at:
http://pig.sagepub.com/content/225/3/347

Published by:

http://www.sagepublications.com

On behalf of:

Institution of Mechanical Engineers

Aeroelastic characteristics of slender wing/bodies with freeplay non-linearities

F Arévalo[1]* and **P García-Fogeda**[2]
[1]Structural Dynamics and Aeroelasticity Department, AIRBUS Military, Getafe, Madrid, Spain
[2]Departamento de Vehículos Aeroespaciales, Universidad Politécnica de Madrid, Madrid, Spain

The manuscript was received on 24 October 2009 and was accepted after revision for publication on 5 July 2010.

DOI: 10.1243/09544100JAERO734

Abstract: This article presents a time domain approach to the flutter analysis of a missile-type wing/body configuration with concentrated structural non-linearities. The missile wing is considered fully movable and its rotation angle contains the structural freeplay-type non-linearity. Although a general formulation for flexible configurations is developed, only two rigid degrees of freedom are taken into account for the results: pitching of the whole wing/body configuration and wing rotation angle around its hinge. An unsteady aerodynamic model based on the slender-body approach is used to calculate aerodynamic generalized forces. Limit-cycle oscillations and chaotic motion below the flutter speed are observed in this study.

Keywords: aeroelasticity, non-linearity, slender wing/body, flexible, freeplay

1 INTRODUCTION

Although the assumption of linearity for both aerodynamics and structural dynamics is often employed in the aeroelastic analysis of missiles, there are many examples where non-linearities exist that can have a significant effect on the aeroelastic response.

Structural non-linearities can be characterized as either *distributed* or *concentrated*, according to their origin. Distributed non-linearities arise from slippage in riveted joints or from buckling in a built-up structure, for example, whereas concentrated non-linearities have a local effect in a control mechanism or an attachment of external stores. Most flight vehicles may have inherently concentrated structural non-linearities such as freeplay, friction, hysteresis, and preload in the hinge part of their control surfaces and folded sections. Concentrated structural non-linearities may be generated from a worn or loose hinge connection of control surface, joint slippage, and manufacturing tolerance. An excellent review of some possible structural non-linearities and their aeroelastic effect are given by Breitbach [**1**] and Woolston *et al.* [**2**]. Among all these several structural non-linearities, the freeplay usually gives the most critical flutter condition. Missile control surfaces that are designed to be easily attached or removed, all-movable aircraft lifting surfaces such as horizontal tails, or rotatable pylons on variable-sweep aircraft exhibit freeplay-type non-linear behaviour that can be potentially dangerous from an aeroelastic standpoint. This article deals with the freeplay non-linearity of a missile control surface.

Aerodynamic non-linearities are important in the transonic regime or stall conditions. Kim and Lee [**3**] analyse a two-degrees-of-freedom airfoil with a freeplay non-linearity in pitch and plunge directions in the transonic and low-supersonic flow regime, using a two-dimensional (2D) unsteady Euler code to calculate unsteady aerodynamic forces. Tang and Dowell [**4**] accounted for aerodynamic stall using the Office National d'Etudes et de Recherches Aérospatiales (French Aeronautics and Space Research Center) (ONERA) model. However, most authors assume linear aerodynamics in the subsonic flow regime, and simplified theories have been used till now. Laurenson and Trn [**5**] use a quasi-steady approach in the sense that the aerodynamic forces are in phase with the motion of a missile control surface, Brase and Eversman [**6**] use a doublet-lattice method, Price *et al.* [**7**] uses incompressible Wagner's function for a 2D airfoil, and O'Neil and Strganac [**8**] model the aerodynamic forces by

*Corresponding author: Structural Dynamics and Aeroelasticity Department, AIRBUS Military, John Lennon s/n, Getafe, Madrid 28906, Spain.
email: felix.arevalo@upm.es; felix.arevalo@casa.eads.net

the aerodynamic theory of Theodorsen for a 2D airfoil. This article uses the slender-body hypothesis so that the subsonic/supersonic unsteady aerodynamic equations are reduced to calculate 2D incompressible flow in planes transverse to the freestream velocity.

Additionally, all the aforementioned studies deal with 2D airfoils or 3D control surfaces with structural non-linearities in pitch or plunge directions. None of them has taken into account wing/body interference when calculating aerodynamic forces. Wing/body configurations can be solved, for arbitrary motions and deformations, by panel methods or computational fluid dynamics (CFD) codes. Panel methods have two main drawbacks: first, for very slender bodies, numerical instabilities occur and the number of panels has to be highly increased; second, the unsteady aerodynamic forces are calculated in the frequency domain but to study non-linear aeroelastic characteristics the time domain is more suitable. For the CFD codes the computational time needed for a single case is yet the main inconvenience. In the first stages of the design process or when the influence of several parameters needs to be evaluated the use of CFD codes can be unaffordable. The application of the slender wing/body theory can provide good results for these first stages of the design process. The unsteady slender-body theory developed here is based on references [**9**] to [**11**]. In these references steady aerodynamic forces are calculated over slender wing/body configurations by means of conformal transformation tools. For unsteady calculations for slender wing/body configurations, the potential equation remains the same as the equation for the steady cases (i.e. 2D transverse flow), what makes valid the same conformal transformations, but boundary conditions are different due to the unsteady motion of the wing/body.

Thus, a wing/body configuration including aerodynamic interference and a non-linearity on the wing control mechanism is analysed in this article by means of unsteady slender-body theory. A typical configuration of the type studied can be seen in Fig. 1. The underwing store or missile on the figure is the only component considered for the analysis.

The missile can be in free-flight or attached to an aircraft. In the last case, the aerodynamic interference between aircraft wing and missile will not be taken into account as a first step. This aerodynamic interference should be negligible for the lateral motion of the missile (mainly lateral and yawing modes of the missile/pylon component). Only for vertical motion of the missile, the wing/missile aerodynamic interference should be assessed. Therefore, the results shown into this article are representative for free-flight condition or attached-to-aircraft configuration undergoing lateral displacements.

The results obtained for the unsteady generalized aerodynamic forces are directly in the time domain and can be coupled with the time domain

(Source: U.S. Defenseimagery.mil photo DF-SC-99-00806/970922-F-0024F-003. Photographer: TSgt. Brad Fallin, USAF
As a work of the U.S. federal government, the image is in the public domain. See http://www.defenselink.mil/multimedia/about.html)

Fig. 1 Typical configuration under the wing

structural equations including any type of structural non-linearity. Limit-cycle oscillations or chaos bands as functions of different parameters can be obtained after numerical integration. Time integration of the equations and discrete Fourier analysis of the response are the tools used to investigate the type of motion that results from particular initial conditions. Although a general formulation is presented (including rigid degrees of freedom plus bending flexible modes), only wing/body pitching and wing rotational angle degrees of freedom are considered in the results.

2 GENERAL FORMULATION

Let one consider an isolated slender wing/body configuration flying at a velocity U_∞ and performing small motion in the z-axis direction transverse to the freestream (see Fig. 2). Wing and body x-constant frames are considered rigid, and the 'z' displacements are defined by an equation that depend on 'x' exclusively

$$w(x;t) = \sum_{i=1}^{N} \psi_i(x) \cdot \xi_i(t) \tag{1}$$

where ψ_i are the modes of vibration (normal modes), including rigid wing/body modes, and ξ_i are the generalized co-ordinates. This displacement $w(x;t)$ is defined positive downwards.

These slender wing/body configurations resemble missiles, in which the wing acts as an aerodynamic control. Therefore, together with the plunging and pitching rigid modes of the complete configuration, the wing may have its own rigid and flexible modes relative to the body. The all-movable wing, which is discussed here, is an example of these kinds of configurations, in which the complete wing rotates around the hinge to control the missile. Nielsen [**9**] describes several types of aerodynamic control surfaces.

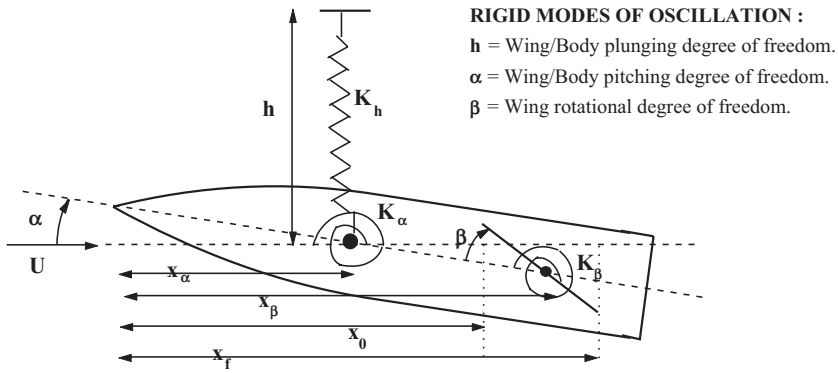

Fig. 2 Slender wing/body configuration flying at velocity U_∞

Plunging and pitching rigid modes of the whole missile configuration can have different physical meanings. For example, they can represent bending and torsion motions of the wing section of the airplane where the missile is attached, or they can represent the airplane wing/missile attachment. This bending/torsion or attachment stiffness is characterized by support springs K_h and K_α (Fig. 2).

Missile wing rigid mode is normally the one associated with rotary motion around the hinge to control the missile. The control mechanism stiffness is represented by the root rotational support spring K_β (Fig. 2).

Concentrated structural non-linearities can be introduced in one or several rigid degrees of freedom, although this article deals with freeplay-type non-linearity associated with the wing control mechanism. This non-linearity might represent a loose hinge, linkage of a control system, or possible joint slippage.

The equations of motion that describe the time evolution of the generalized co-ordinates are obtained using Lagrange's equations

$$\frac{\mathrm{d}}{\mathrm{d}t}\left(\frac{\partial T}{\partial \dot{\xi}_i}\right) - \frac{\partial T}{\partial \xi_i} + \frac{\partial U}{\partial \xi_i} = Q_i, \quad i = 1, 2, \ldots, N \tag{2}$$

where T is the kinetic energy, U is the strain energy, Q_i is the generalized aerodynamic force corresponding to the generalized co-ordinate ξ_i, and N is the number of modes.

3 INERTIA, STIFFNESS, AND AERODYNAMIC LOAD CALCULATION

In this section, Langrange's equations are written in matrix notation.

3.1 Inertia loads

Inertia loads result from deriving the kinetic energy with respect to the first time derivative of the generalized co-ordinates. Kinetic energy expressed as a function of the generalized co-ordinates is

$$T = \sum_{i=1}^{N}\sum_{j=1}^{N}\left(\int_0^L \frac{1}{2} m(x)\psi_i(x)\psi_j(x)\,\mathrm{d}x\right)\dot{\xi}_i\,\dot{\xi}_j \tag{3}$$

where $m(x)$ is the wing/body mass per unit length, L is the total length, and N is the number of modes. If one of the modes corresponds to the wing motion/bending relative to the body, the integration is extended exclusively to the wing, with $m(x)$ being the wing mass per unit length.

From this it follows that

$$\frac{\mathrm{d}}{\mathrm{d}t}\left(\frac{\partial T}{\partial \dot{\xi}_i}\right) = \sum_{j=1}^{N} J_{ij}\,\ddot{\xi}_j \tag{4}$$

where $J_{ij} = \int_0^L m(x)\psi_i(x)\psi_j(x)\,\mathrm{d}x$

In matrix notation, with all the generalized co-ordinates ordered in a column, it can be written as

$$\begin{bmatrix} J_{11} & J_{12} & \cdots & J_{1N} \\ J_{21} & J_{22} & \cdots & J_{2N} \\ \vdots & \vdots & & \vdots \\ J_{N1} & J_{N2} & \cdots & J_{NN} \end{bmatrix} \begin{Bmatrix} \ddot{\xi}_1 \\ \ddot{\xi}_2 \\ \vdots \\ \ddot{\xi}_N \end{Bmatrix} = [\mathbf{J}] \cdot \{\ddot{\xi}\} \tag{5}$$

3.2 Stiffness matrix

Stiffness loads result from deriving the strain energy with respect to the generalized co-ordinates. Strain

energy is expressed as a function of the generalized co-ordinates as follows

$$U = U_{\text{rigid}} + U_{\text{flexible}} = \sum_{i=1}^{M} \frac{1}{2} K_i \xi_i^2 + \sum_{i=1}^{N} \sum_{j=1}^{N} \left(\int_0^L \frac{1}{2} EI(x) \psi_i'' \psi_j'' \, \mathrm{d}x \right) \xi_i \xi_j \tag{6}$$

where U_{rigid} is the strain energy associated to the springs attached to the wing/body rigid degrees of freedom (those that simulate external actions over the wing and/or body component) and U_{flexible} the strain energy associated with the wing/body bending flexible modes. $EI(x)$ is the flexural rigidity and M is the number of rigid modes. As aforementioned, three rigid degrees of freedom are going to be considered: plunging, pitching of the whole wing/body configuration, and the rotary degree of freedom of the wing as aerodynamic control.

If one of the modes corresponds to the wing motion/bending relative to the body, the integration is extended exclusively to the wing, with $EI(x)$ being the wing stiffness.

From this it follows that

$$\frac{\partial U}{\partial \xi_i} = K_i \xi_i + \sum_{j=1}^{N} K_{ij} \xi_j \tag{7}$$

where $K_{ij} = \int_0^L EI(x) \psi_i'' \psi_j'' \, \mathrm{d}x$

In matrix notation, with all the generalized co-ordinates ordered in a column

$$\begin{bmatrix} K_1 & K_{12} & \cdots & K_{1N} \\ K_{21} & K_2 & \cdots & K_{2N} \\ \vdots & \vdots & & \vdots \\ K_{N1} & K_{N2} & \cdots & K_{NN} \end{bmatrix} \begin{Bmatrix} \xi_1 \\ \xi_2 \\ \vdots \\ \xi_N \end{Bmatrix} = [\mathbf{K}] \cdot \{\xi\} \tag{8}$$

where K_{ii} is zero if i is a rigid mode.

3.3 Aerodynamic generalized forces

The slender wing/body theory is applied for the computation of the unsteady aerodynamic forces. The theory is formulated so that rigid and flexible wing/body modes can be considered and the generalized co-ordinates are kept in the time domain. In this way, a full set of equilibrium equations in the time domain are obtained for the numerical integration.

Aerodynamic generalized forces over wing and body components are obtained as follows

$$Q_{ij}^{\text{B}} = q_\infty \int_0^L \int_0^{2\pi} C_{pj}^{\text{B}}(x, \theta; t) R(x) \sin\theta \, \psi_i(x) \, \mathrm{d}\theta \, \mathrm{d}x \tag{9}$$

$$Q_{ij}^{\text{W}} = q_\infty \iint_{S_w} \Delta C_{pj}^{\text{w}}(x, y; t) \psi_i(x) \, \mathrm{d}x \, \mathrm{d}y \tag{10}$$

where

$Q_{ij}^{\text{B}} = i$th-mode generalized force induced by the jth mode of deflection
$Q_{ij}^{\text{W}} = i$th-mode generalized force induced by the jth mode of deflection
$q_\infty =$ dynamic pressure
$C_{pj}^{\text{B}} =$ unsteady pressure coefficient over body induced by mode of deflection j
$\Delta C_{pj}^{\text{w}} =$ unsteady pressure coefficient over wing induced by mode of deflection j
$R(x) =$ body radius

The total generalized forces over the wing/body configuration are obtained by adding wing and body contributions

$$Q_{ij} = Q_{ij}^{\text{W}} + Q_{ij}^{\text{B}} \tag{11}$$

The pressure coefficient depends linearly on the generalized co-ordinates, and the generalized force Q_{ij} can be written as

$$Q_{ij} = q_\infty \{ A_{\xi_i \xi_j} \xi_j + A_{\xi_i \dot{\xi}_j} \dot{\xi}_j + A_{\xi_i \ddot{\xi}_j} \ddot{\xi}_j \} \tag{12}$$

The generalized aerodynamic force is then

$$Q_i = \sum_{j=1}^{N} Q_{ij} \tag{13}$$

In matrix notation

$$\{\mathbf{Q}\} = q_\infty \{ [\mathbf{A}_{\xi\xi}]\{\xi\} + [\mathbf{A}_{\xi\dot{\xi}}]\{\dot{\xi}\} + [\mathbf{A}_{\xi\ddot{\xi}}]\{\ddot{\xi}\} \} \tag{14}$$

Unsteady pressure coefficient distributions are calculated by assuming slender wing/body configuration. This hypothesis is fulfilled in missile configurations just as the ones analysed in this article. Section 4 details the slender-body theory on its application to unsteady flow.

4 PRESSURE COEFFICIENT DISTRIBUTIONS

Pressure coefficient requires solving the velocity field around the configuration. Slender configuration hypothesis simplifies this calculation reducing the compressible 3D flow to incompressible 2D.

4.1 Potential flow over slender wing/body configuration

The fluid flow is assumed to be inviscid and isentropic. Thus, the fluid velocity can be defined by the scalar potential $\Omega(x, y, x; t)$. In a body-fixed reference system [**12**], this potential is written as

$$\hat{\Omega}(\hat{x}, \hat{y}, \hat{z}; \hat{t}) = \hat{x} + \frac{\partial \hat{w}(\hat{x}; \hat{t})}{\partial \hat{x}} \hat{z} + \hat{\Phi}(\hat{x}, \hat{y}, \hat{x}; \hat{t}) \tag{15}$$

where $\hat{\Phi}(\hat{x}, \hat{y}, \hat{z}; \hat{t})$ is the non-dimensional perturbation potential and $\hat{w}(\hat{x}; \hat{t})$ is the instantaneous non-dimensional wing/body z-displacement. The

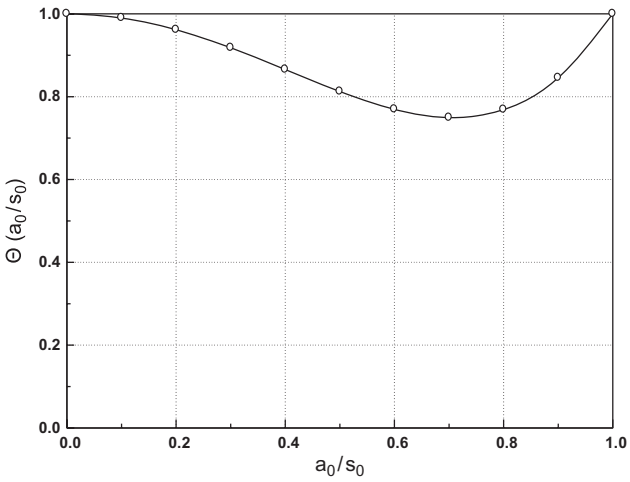

Fig. 3 Comparison of the Θ function between the present method and that of Sacks [**13**]

wing/body configuration length L and the fluid velocity at infinity U_∞ are the reference magnitudes used to build non-dimensional variables. The perturbation potential is split into two parts: the mean zero-angle-of-attack potential flow $\hat{\phi}_0$ and the unsteady potential $\hat{\phi}_1$, i.e.

$$\hat{\Phi}(\hat{x},\hat{y},\hat{z};\hat{t}) = \hat{\phi}_0(\hat{x},\hat{y},\hat{z}) + \hat{\phi}_1(\hat{x},\hat{y},\hat{z};\hat{t}) \tag{16}$$

Substituting the previous expression for the potential in the full potential equation, and collecting terms of the same order of magnitude

$$\left(1-M_\infty^2\right)^2 \frac{\partial^2\hat{\phi}_0}{\partial\hat{x}^2} + \frac{\partial^2\hat{\phi}_0}{\partial\hat{y}^2} + \frac{\partial^2\hat{\phi}_0}{\partial\hat{z}^2} = 0 \tag{17}$$

$$\left(1-M_\infty^2\right)\frac{\partial^2\hat{\phi}_1}{\partial\hat{x}^2} + \frac{\partial^2\hat{\phi}_1}{\partial\hat{y}^2} + \frac{\partial^2\hat{\phi}_1}{\partial\hat{z}^2} - 2M_\infty^2\frac{\partial^2\hat{\phi}_1}{\partial\hat{x}\partial\hat{t}} - M_\infty^2\frac{\partial^2\hat{\phi}_1}{\partial\hat{t}^2} = F(\hat{x},\hat{z},\hat{w},\hat{\phi}_0,M_\infty;t) \tag{18}$$

Table 1 Geometrical characteristic and other parameters of the wing/body configuration of Fig. 1

Body radius	$\hat{R}(\hat{x}) = 2\tau\hat{x}(1-\hat{x})$ if $0 \leqslant \hat{x} \leqslant 0.5$, and $R(\hat{x}) = \tau/2$ if $\hat{x} \geqslant 0.5$; $\tau = 0.1$
Centre of wing/body rigid pitching mode	$\hat{x}_\alpha = 0.5$
Wing	Sweep: 30°
	Position relative to the body: $\hat{x}_0 = 0.75; \hat{x}_f = 0.95$
	Hinge position: $\hat{x}_\beta = \hat{x}_0 + 3(\hat{x}_f - \hat{x}_0)/4$
Stiffness and mass properties	Rigid modes natural frequencies: $\omega_h/\omega_0 = 1.0$, $\omega_\alpha/\omega_0 = 1.0$, $\omega_\beta/\omega_0 = 2.0$
	Mass parameter $\mu = 1.0$
Freeplay dead space band (degrees)	$[-0.1, 0.1]$
Initial conditions for integration	$\alpha(0) = \dot{\alpha}(0) = \dot{\beta}(0) = 0$, $\beta(0) = 0.1°$

Dimensions are non-dimensionalized by the wing/body length L.

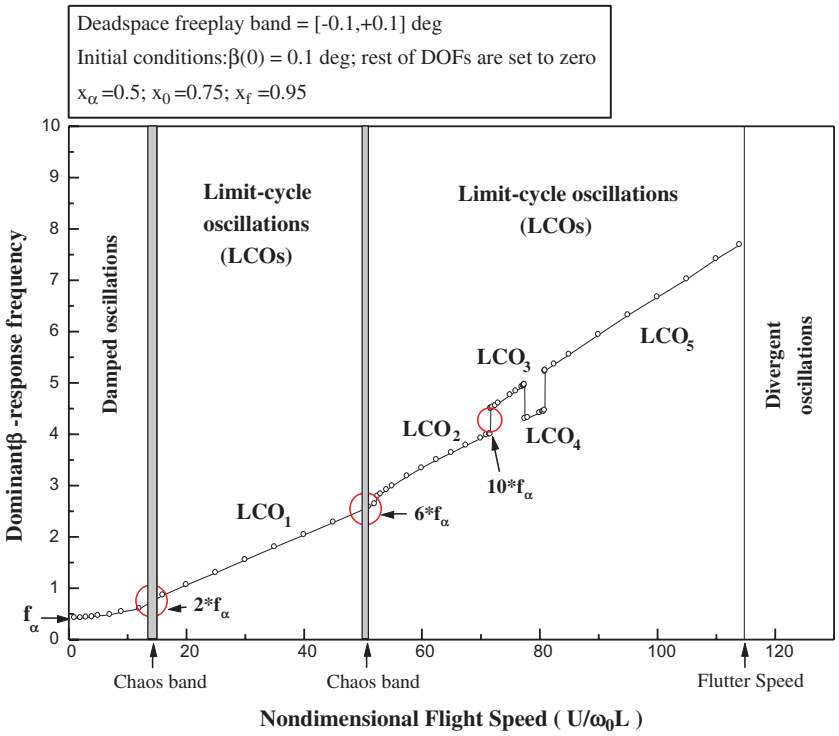

Fig. 4 Dominant frequency of the β time history (from discrete Fourier analysis) versus non-dimensional flight speed

two equations for the potentials $\hat{\phi}_0$ and $\hat{\phi}_1$ are obtained. For a slender wing/body configuration, it is shown [**9**] that both previous equations are reduced to

$$\frac{\partial^2 \hat{\phi}_0}{\partial \hat{y}^2} + \frac{\partial^2 \hat{\phi}_0}{\partial \hat{z}^2} = 0 \tag{19}$$

$$\frac{\partial^2 \hat{\phi}_1}{\partial \hat{y}^2} + \frac{\partial^2 \hat{\phi}_1}{\partial \hat{z}^2} = 0 \tag{20}$$

These equations are known to correspond to a disturbed flow of an incompressible fluid in the plane $\hat{y}\hat{z}$.

The mean flow equation has the following solution for axisymmetric bodies that fulfils the boundary condition of tangency over the wing/body surface and zero disturbance velocity at infinity

$$\hat{\phi}_0(\hat{x}, \hat{r}) = \hat{R}(\hat{x}) \frac{\mathrm{d}\hat{R}(\hat{x})}{\mathrm{d}\hat{x}} \ln \sqrt{\hat{y}^2 + \hat{z}^2} + g(\hat{x}, M_\infty) \tag{21}$$

where $\hat{R}(\hat{x})$ is the dimensionless body radius.

The equation for the unsteady potential $\hat{\phi}_1$ must be solved with the boundary condition of tangency over the body surface and the following velocity at infinity

$$\frac{\partial \hat{\phi}_1}{\partial \hat{z}} = \frac{\partial \hat{w}}{\partial x} + \frac{\partial \hat{w}}{\partial \hat{t}} \tag{22}$$

This problem of 2D incompressible flow with a boundary condition at infinity can be solved using the theory of *conformal transformation*. This conformal transformation will depend of the tangency boundary condition at the wing/body surface. Both Nielsen [**9**] and Krasnov [**10**] solve the problem of the wing/body configuration with wing and body moving together (fixed wing), and Nielsen [**9**] solves the problem of wing/body configuration with the wing having a motion relative to the body (wing as aerodynamic control). Although these authors solve the steady problem for rigid wing/body configuration, the unsteady one for flexible wing/body configuration

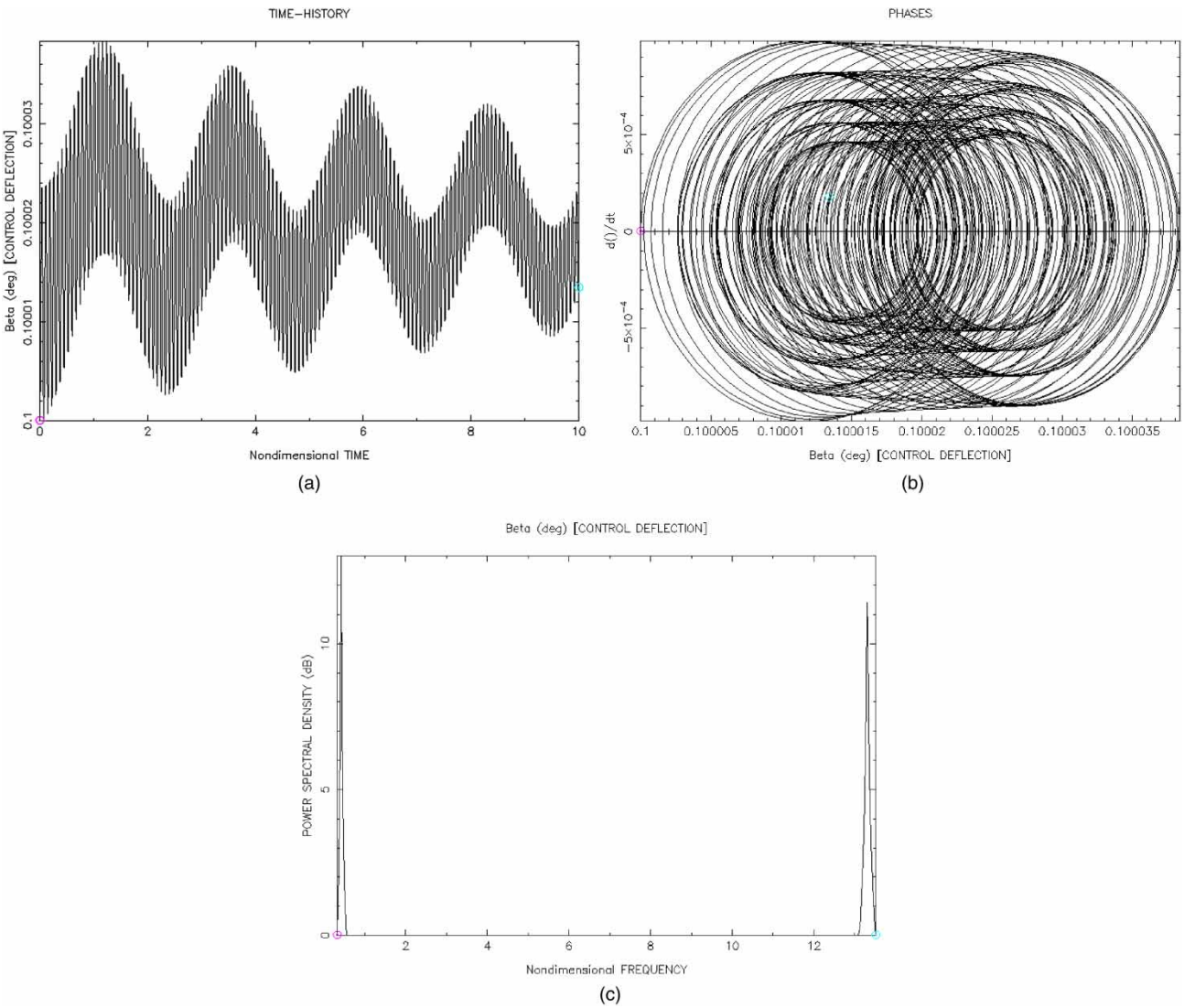

Fig. 5 Non-dimensional velocity 2.00: (a) β time history, (b) β phase diagram, and (c) discrete Fourier analysis of β time history. Characteristic frequencies are 0.42, 13.25

is similar except for updating the infinity boundary condition by equation (22).

4.2 Unsteady pressure coefficient

Integration of the zero angle-of-attack pressure coefficient distribution C_{p0} results in zero total aerodynamic force/moment over the entire configuration. The unsteady pressure coefficient is obtained from the following equation

$$C_{p1}(\hat{x},\hat{y};\hat{t}) = -2\left[\left(1+\frac{\partial\hat{\phi}_0}{\partial\hat{x}}\right)\left(\frac{\partial\hat{\phi}_1}{\partial\hat{x}} - \hat{z}\frac{\partial^2\hat{w}}{\partial\hat{x}^2}\frac{\partial\hat{\phi}_0}{\partial\hat{x}}\right) + \frac{\partial\hat{\phi}_0}{\partial\hat{z}}\left(\frac{\partial\hat{\phi}_1}{\partial\hat{z}} + \frac{\partial\hat{w}}{\partial\hat{x}}\right) + \frac{\partial\hat{\phi}_0}{\partial\hat{y}}\frac{\partial\hat{\phi}_1}{\partial\hat{y}} + \frac{\partial\hat{\phi}_1}{\partial\hat{t}} + \frac{\partial\hat{w}}{\partial\hat{t}}\frac{\partial\hat{\phi}_0}{\partial\hat{z}} - \hat{z}\frac{\partial^2\hat{w}}{\partial\hat{x}\partial\hat{t}}\frac{\partial\hat{\phi}_0}{\partial\hat{x}}\right] \tag{23}$$

This pressure coefficient is substituted in Equations (9) and (10) to calculate the aerodynamic generalized forces.

The unsteady aerodynamic forces have been validated by comparing the stability derivatives for the wing/body configuration of reference [**13**]. A unique function Θ for all stability derivatives can be defined as

$$\Theta\left(\frac{a_0}{s_0}\right) = \frac{C_{L\alpha}}{(\pi/2)A} = \frac{C_{Lq}}{(\pi/6)A} = \frac{C_{L\dot{\alpha}}}{(\pi/6)A} = -\frac{C_{M\alpha}}{(\pi/72)A} = -\frac{C_{Mq}}{(\pi/24)A} \tag{24}$$

where a_0 is the body radius at the base and s_0 is the semi-span of the triangular wing.

The results for this function are compared with those obtained by Sacks [**13**] in Fig. 3. The solid line is Sack's results and the dots are the ones obtained by the present code.

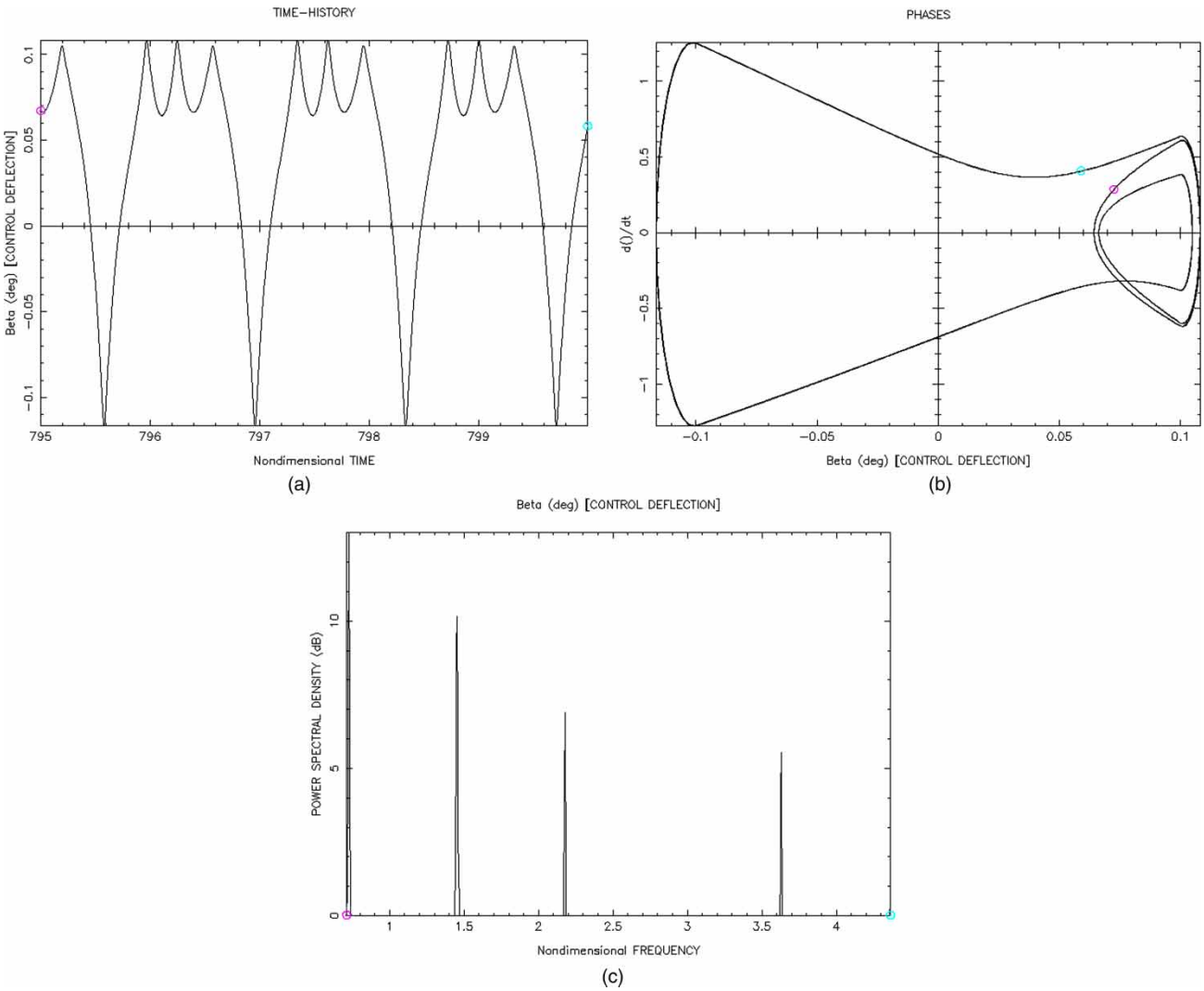

Fig. 6 Non-dimensional velocity 13.00: (a) β time history, (b) β phase diagram, and (c) discrete Fourier analysis of β time history. Characteristic frequencies are 0.727, 1.453, 2.177, 3.630, and 4.360

5 NON-DIMENSIONAL MATRIX FORMULATION OF LAGRANGE'S EQUATIONS

Next by coupling the generalized unsteady aerodynamic forces with the structural equations, the following system of equations describe the time evolution of the generalized co-ordinates with time

$$[\mathbf{J}]\left\{\frac{\mathrm{d}^2\xi}{\mathrm{d}t^2}\right\}+[\mathbf{K}]\{\xi\}=q_\infty\left\{[\mathbf{A}_{\xi\xi}]\{\xi\}+[\mathbf{A}_{\xi\dot{\xi}}]\left\{\frac{\mathrm{d}\xi}{\mathrm{d}t}\right\}+[\mathbf{A}_{\xi\ddot{\xi}}]\left\{\frac{\mathrm{d}^2\xi}{\mathrm{d}t^2}\right\}\right\} \tag{25}$$

Ordering this equation and using non-dimensional parameters it is obtained

$$\left([\hat{\mathbf{J}}]-\frac{1}{2\pi\mu}[\hat{\mathbf{A}}_{\xi\ddot{\xi}}]\right)\left\{\frac{\mathrm{d}^2\hat{\xi}}{\mathrm{d}t^2}\right\}-\frac{(U_\infty/\omega_0 L)}{2\pi\mu}[\hat{\mathbf{A}}_{\xi\dot{\xi}}]\left\{\frac{\mathrm{d}\hat{\xi}}{\mathrm{d}\hat{t}}\right\}+\left([\hat{\mathbf{K}}]-\frac{(U_\infty\omega_0 L)^2}{2\pi\mu}[\hat{\mathbf{A}}_{\xi\xi}]\right)\{\hat{\xi}\}=0 \tag{26}$$

where: $\hat{t}=\omega_0 t$ = dimensionless time; $\hat{\xi}$ = dimension less generalized co-ordinate ξ/L; ω_0 = reference frequency, normally the natural frequency of rigid wing/body pitching vibration in vacuum is chosen in the literature; $\mu=m_0/\pi\rho_\infty L^2$ = density ratio, with m_0 the reference mass per unit length, L the wing/body configuration length, and ρ_∞ the air density at flight level.

This system of equations is numerically integrated, yielding the system time history response information. System stability characteristics are then obtained by evaluating the nature of this system response. The integration method is validated, without the structural non-linearities, by comparing linear flutter velocities with those obtained by the V–g method. Once linear flutter is obtained, structural non-linearities are introduced into the system and time histories are plotted.

Concentrated structural non-linearities will be simulated through the stiffness matrix [**K**]. As

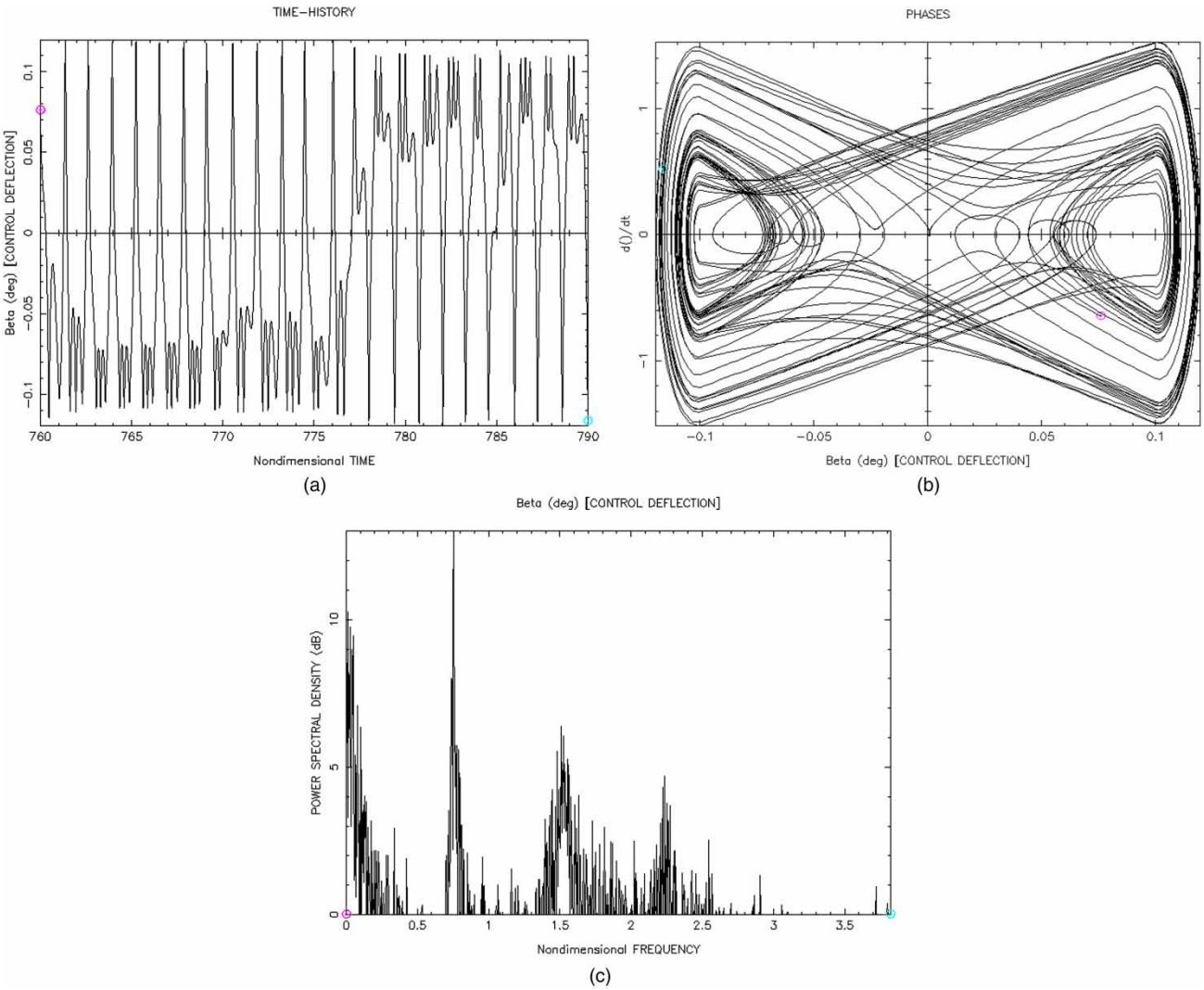

Fig. 7 Non-dimensional velocity 14.00: (a) β time history, (b) β phase diagram, and (c) discrete Fourier analysis of β time history. Chaos without characteristic frequencies

mentioned above, non-linearity is associated with freeplay, or 'slop', in the root support stiffness of the wing. It will be shown that this non-linear approach, where V–g method fails, can detect strange behaviour of the system below the linear flutter speed.

6 RESULTS

A simplified two-degrees-of-freedom wing/body configuration is the basis for the calculation of the following results (Fig. 2). The two modes that correspond to the mentioned degrees of freedom are the following:

(a) wing/body angle of attack, α: pitching rigid mode of the whole wing/body configuration, positive in the nose-up direction, $\hat{\psi}_1 = \hat{x} - \hat{x}_\alpha$;

(b) wing rotation angle, β: wing rotation around the hinge $\hat{x}_\beta$ as an aerodynamic control, positive when leading edge moves up, $\hat{\psi}_2 = \hat{x} - \hat{x}_\beta$.

Neither the plunging rigid mode of the whole wing/body configuration nor flexible modes are considered here in order to reduce the number of unknown sources than determine the solution pattern. Further studies will include the effect of these modes.

Flutter without structural non-linearities has been obtained for checking purposes. V–g method supplies flutter speeds that have been validated by time integration of the equations.

After that, freeplay-type non-linearity is introduced in the wing rotational degree of freedom β. Table 1 summarizes the main dimensions of the wing/body configuration together with other properties of the system (mass parameter value, initial conditions, etc.).

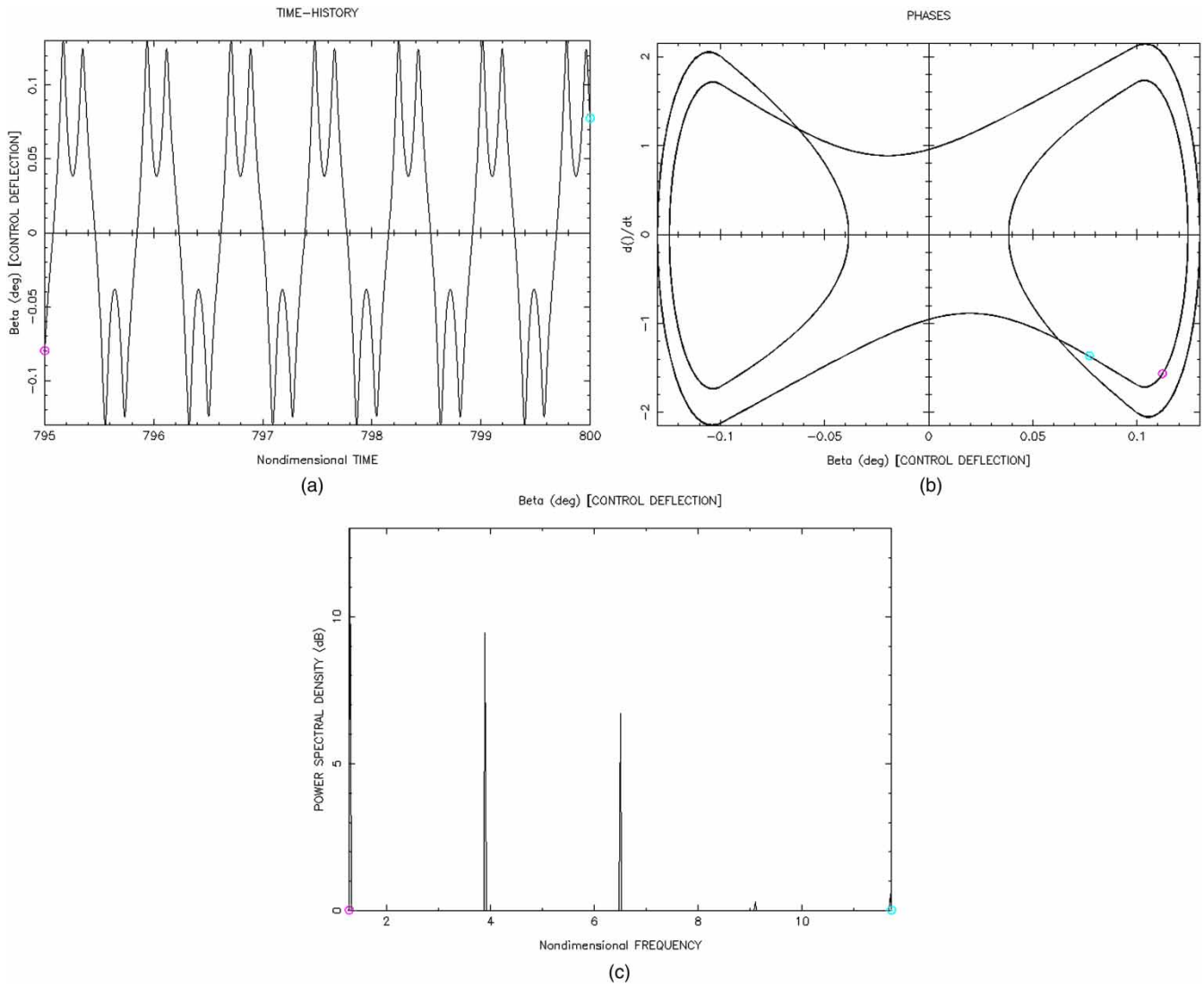

Fig. 8 Non-dimensional velocity 25.00: (a) β time history, (b) β phase diagram, and (c) discrete Fourier analysis of β time history. Characteristic frequencies are 1.300, 3.900, 6.507, and 11.707

To avoid instability in the numerical integration when passing from one linear region to another in the freeplay type of non-linearity, Conner *et al.* [**14**] have shown that the application of Henon's method has many advantages. For the results presented in this article the method of reference [**14**] has been adopted.

Equation (26) is integrated using the non-dimensional flight speed $U_\infty/\omega_0 L$ as a parameter. Figures 5 to 11 show time histories (a), phase diagram (b), and power spectral densities (c) of the wing control deflection β for several values of the non-dimensional speed. Figure 4 shows the dominant frequency of the β time history as a function of the non-dimensional flight speed. Initial conditions are zero angle of attack and 0.1° for β deflection.

Starting from zero, the non-dimensional flight speed is increased. Damped oscillations (Fig. 5(a)) are obtained till the non-dimensional speed of 13 is reached (Fig. 6(a)), where both degrees of freedom α and β develop no-damped limit-cycle oscillations. The β phase diagram with a closed orbit in 0.1° shows that β suffers short-time oscillations around 0.1°.

Immediately after this speed, there appears a band of chaotic motion from 13.5 to 15 non-dimensional flight speed (Fig. 7(a)). The wing control deflection β jumps arbitrarily from −0.1° to 0.1°, with short-time oscillations between two jumps. The chaos-type response is detected by the appearance of a broad-band power spectral density (PSD) without dominant frequencies of the β time history (Fig. 7(a)) and a phase diagram (Fig. 7(b)) without defined attractor points (*strange attractors* in the nomenclature of non-linear dynamics).

After this chaotic band, a new type of limit-cycle oscillation (LCO_1 in Fig. 4) appears for non-dimensional speeds from 15 to 49. This is characterized in the phase diagram of Fig. 8(b) by a configuration

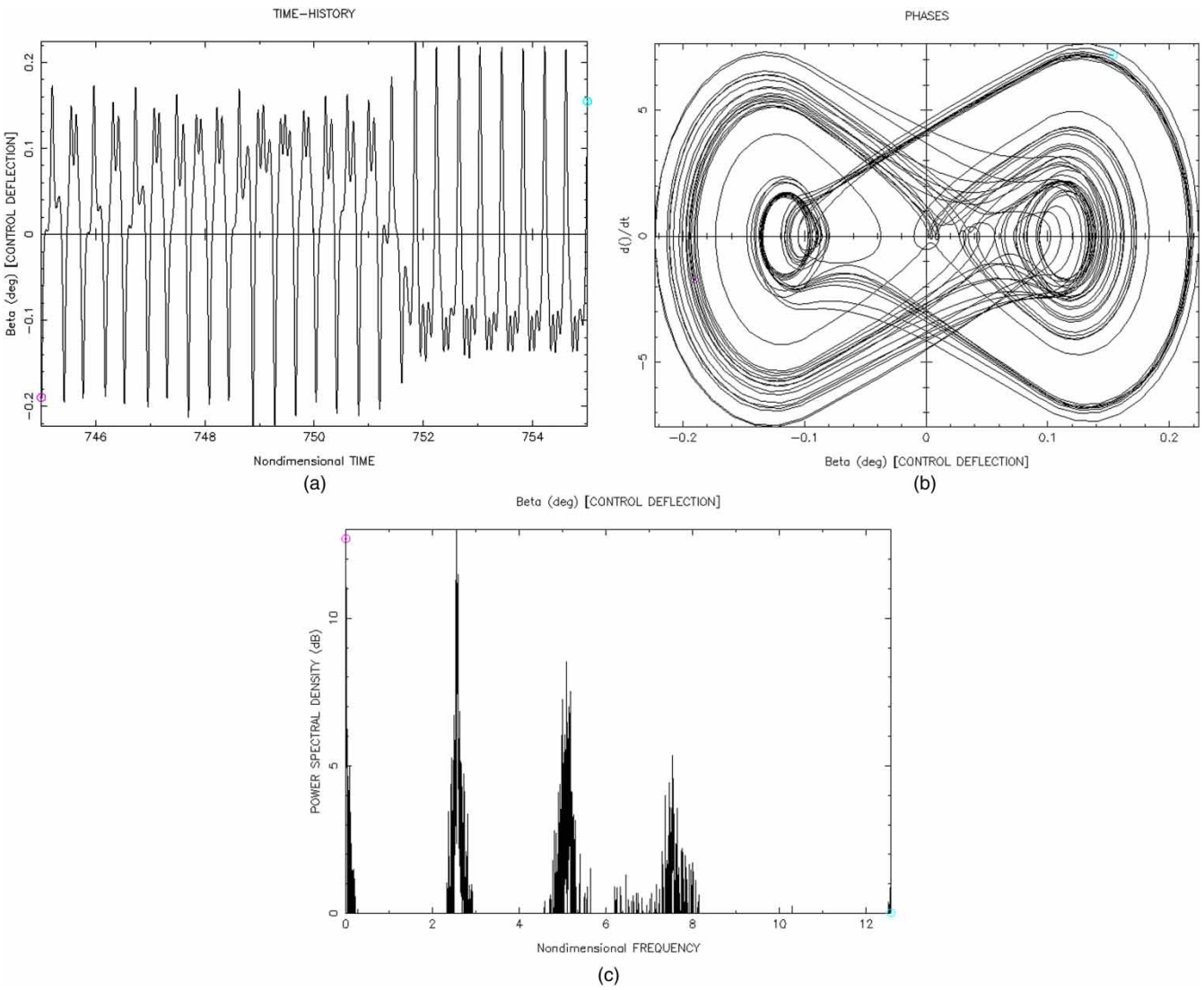

Fig. 9 Non-dimensional velocity 50.00: (a) β time history, (b) β phase diagram, and (c) discrete Fourier analysis of β time history. Chaos without characteristic frequencies

with two closed orbits (two fixed points), showing that β oscillates around 0.1° or −0.1° before jumping to −0.1° or 0.1°, respectively.

A new chaotic band appears from 49 to 51 non-dimensional speeds. β wing control deflection develops chaotic jumps from −0.1° to 0.1° and dominant characteristic frequencies do not exist as the power spectral density plot shows (Fig. 9(c)).

From the non-dimensional speed to the flutter speed, successive limit-cycle oscillations determine the β response. A first limit-cycle oscillation (LCO_2 in Fig. 4) consists of jumps from −0.1° to 0.1° with short-time double oscillations around 0.1° (Fig. 10(a)). This explains the closed orbit of the phase diagram around 0.1° (Fig. 10(b)). The same occurs with the limit-cycle oscillation LCO_4 (Fig. 4) but with the short-time double oscillations around −0.1°. The other two limit-cycle oscillations (LCO_3 and LCO_5 in Fig. 4) consist of sinusoidal oscillations from −0.1° to 0.1°. Finally, flutter velocity is obtained at the linear flutter speed (i.e. the flutter speed without structural non-linearities (Figs 11(a) to (c))).

The frequencies in aeroelastic systems depend upon aerodynamic pressures. In fact, the dominant frequency of the β response increases with the non-dimensional speed (Fig. 4). The system frequencies may become tuned with a natural frequency of the system (or a multiple) as a consequence of the aerodynamic effects. The natural frequency of the pitching mode (i.e. in the absence of freestream velocity), is 0.42 (frequency labelled f_α in Fig. 4). It can be seen from Fig. 4 that the β-response pattern changes occur when the aeroelastic frequency crosses through particular multiples of the pitching mode natural frequency.

Initial conditions are also important in the response pattern. It has been observed that changing the initial wing/body angle of attack $\alpha(0)$, the chaotic behaviour obtained for a non-dimensional speed of

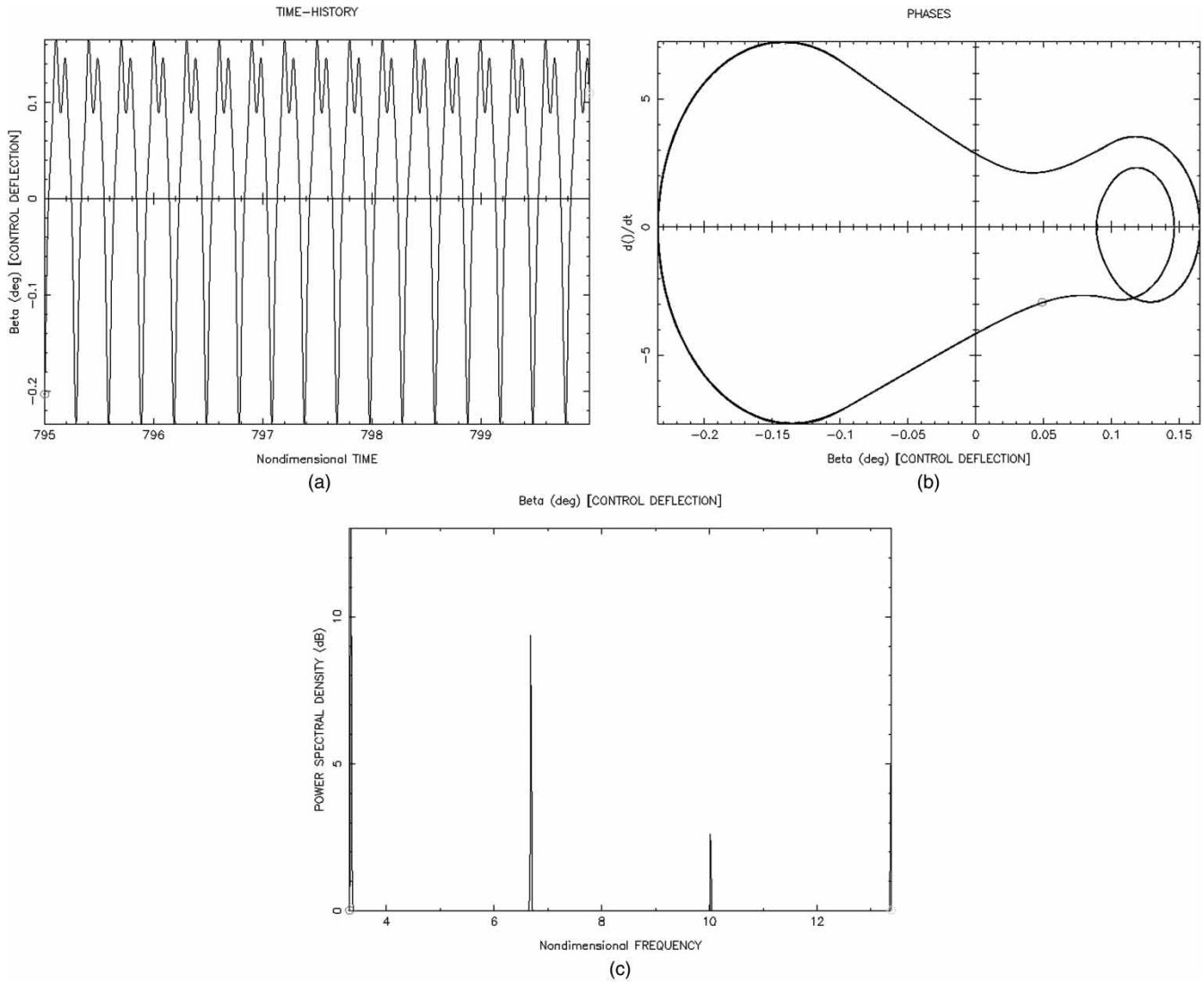

Fig. 10 Non-dimensional velocity 60.00: (a) β time history, (b) β phase diagram, and (c) discrete Fourier analysis of β time history. Characteristic frequencies are 3.340, 6.680, 10.020, and 13.370

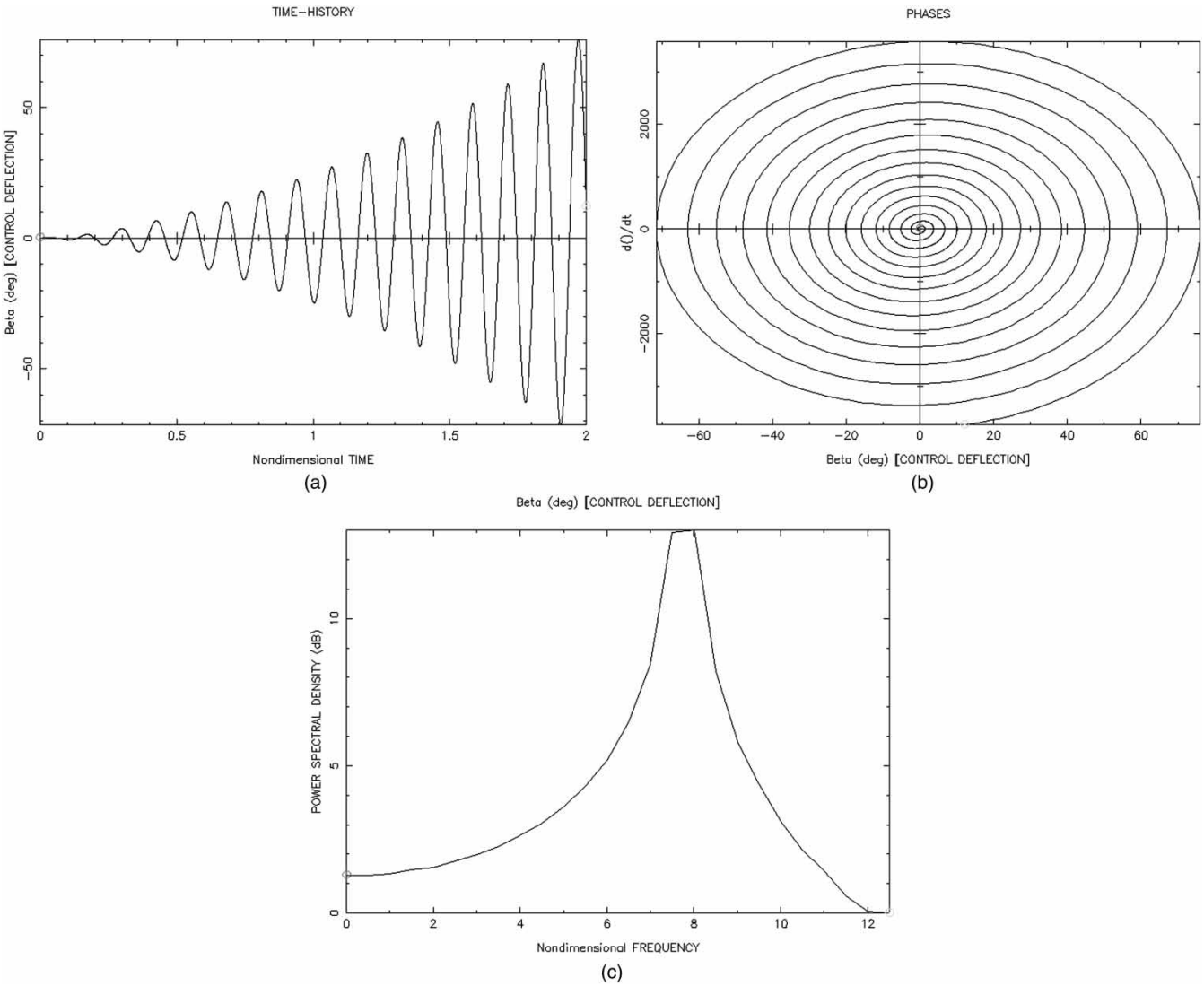

Fig. 11 Non-dimensional velocity 115.00: (a) β time history, (b) β phase diagram, and (c) discrete Fourier analysis of β time history. Characteristic frequencies are 8.800

50 disappears. In fact, this chaotic motion was sustained for all initial $\beta(0)$ when $\alpha(0)$ was less than 0.15°. If $\alpha(0)$ was greater than 0.15° the chaotic behaviour was substituted by a limit-cycle oscillation motion.

Other wing/body configuration with the wing in a forward position has been tested. The response pattern appears to be similar to that observed in Fig. 4 for wing in the rear position, except that the chaotic bands are changed to other non-dimensional speed ranges.

7 CONCLUSIONS

The present study deals with the time domain aeroelastic analysis for a missile-type wing/body configuration with concentrated structural non-linearities. The missile can be in free-flight or attached to the aircraft. In the last case, only lateral motions of the missile are considered since the aerodynamic interference between aircraft wing and missile has not been included at this stage.

The method used in this study can be applied to arbitrarily shape flexible wing/body configurations with multiple non-linearities. A typical missile-type configuration with freeplay non-linearity in the wing control mechanism is selected for numerical simulation. An unsteady slender-body theory is applied to take into account the wing/body aerodynamic interference.

Non-linear flutter analysis shows that limit-cycle oscillations and chaotic motion appear below the flutter speed. Increasing the flight speed the aeroelastic frequency of the response increases, and response pattern changes occur when this frequency is tuned with particular multiples of the wing/body pitching mode natural frequency. Initial conditions modify the results and chaotic behaviour changes to limit-cycle

oscillations when the initial angle of attack of the wing/body configuration is greater than a particular value. Wing position relative to the body also causes similar effects.

Divergent oscillations are obtained above the same flight speed than the equivalent linear system (i.e. the linear flutter speed).

Further developments will include a more detailed study of the system sensibility to the initial conditions, wing/body configuration parameters (wing shape, wing position relative to the body, and so on), flexible modes, and possible non-linearities in other degrees of freedom.

REFERENCES

1 **Breitbach, E.** Effects of structural nonlinearities on aircraft vibration and flutter. In Proceedings of the 45th Structures and Materials AGARD Panel Meeting, AGARD Report 665, Voss, Norway, 1977.

2 **Woolston, D. S., Runyan, H. L.,** and **Andrews, R. E.** An investigation of certain types of structural, nonlinearities on wing and control surface flutter. *J. Aeronaut. Sci.*, 1957, **24**(1), 57–63.

3 **Kim, S.-H.** and **Lee, I.** Aeroelastic analysis of a flexible airfoil with a freeplay nonlinearity. *J. Sound Vibr.*, 1995, **193**(4), 823–846.

4 **Tang, D. M.** and **Dowell, E. H.** Flutter and stall response of a helicopter blade with structural nonlinearity. *J. Aircr.*, 1992, **29**(5), 953–960.

5 **Laurenson, R. M.** and **Trn, R. M.** Flutter analysis of missile control surfaces containing structural nonlinearities. *AIAA J.*, 1980, **18**(10), 1245–1251.

6 **Brase, L. O.** and **Eversman, W.** Application of transient aerodynamics to the structural nonlinear flutter problem. *J. Aircr.*, 1988, **25**(11), 1060–1068.

7 **Price, S. J., Lee, B. H. K.,** and **Alighanbari, H.** Postinstability behaviour of a two-dimensional airfoil with a structural nonlinearity. *J. Aircr.*, 1994, **31**(6), 1395–1401.

8 **O'Neil, T.** and **Strganac, T. W.** Aeroelastic response of a rigid wing supported by nonlinear springs. *J. Aircr.*, 1998, **35**(4), 616–622.

9 **Nielsen, J. N.** *Missile aerodynamics*, 1960 (McGraw-Hill Book Company).

10 **Krasnov, N. F.** *Aerodynamics, methods of aerodynamic calculations (II)*, 1980 (Mir Publishers, Moscow).

11 **Dugan, D. W.** and **Hikido, K.** Theoretical investigation of the effects upon lift of a gap between wing and body of a slender wing-body combination. NACA TN 3224, 1954.

12 **Hoffman, G.** and **Platzer, M. F.** On supersonic flow past oscillating bodies of revolution. *AIAA J.*, 1966, **4**(2), 370.

13 **Sacks, A. H.** Aerodynamic forces and stability derivatives for slender bodies of general cross sections. NACA TN 3283, November 1954.

14 **Conner, M. D., Virgin, L. N.,** and **Dowell, E. H.** Accurate numerical integration of state/space models for aeroelastic systems with free play. *AIAA J.*, 1996, **34**, 2202–2205.